

Detecting the topological edge states by the entanglement convertibility in a local scale of the one-dimensional XXZ model with bond alternation

Yu-Chin Tzeng, Li Dai, and Ming-Chiang Chung

Department of Physics, National Chung Hsing University, Taichung, Taiwan

Luigi Amico

*CNR-MATIS-IMM & Dipartimento di Fisica e Astronomia, Università di Catania,
& INFN-Laboratori Nazionali del Sud, Via S. Sofia 64, 95127 Catania (Italy) and*

Centre for Quantum Technologies, National University of Singapore, 3 Science Drive 2, Singapore 117543

Leong-Chuan Kwek

*Centre for Quantum Technologies, National University of Singapore, 3 Science Drive 2, Singapore 117543, Singapore
Institute of Advanced Studies, Nanyang Technological University, 60 Nanyang View, Singapore 639673, Singapore*

National Institute of Education, Nanyang Technological University,

1 Nanyang Walk, Singapore 637616, Singapore and

MajuLab, CNRS-UNS-NUS-NTU International Joint Research Unit, UMI 3654, Singapore

(Dated: June 14, 2022)

The entanglement convertibility between two quantum pure states is characterized by the Rényi entropy of the reduced state of the subsystem. By means of the density matrix renormalization group, we numerically study the entanglement convertibility and the topological edge states in the spin-1/2 XXZ model with bond alternation, $H = \sum_{n=1}^N [1 + (-1)^n \delta] (\sigma_n^x \sigma_{n+1}^x + \sigma_n^y \sigma_{n+1}^y + \Delta \sigma_n^z \sigma_{n+1}^z)$, within periodic boundary conditions. It is found that for both cases of varying Δ and δ , the convertibility regarding a generic subsystem size L_A in the topological Haldane dimer phase is universally negative. The negative convertibility is attributed to the recombination of edge states which occurs for small L_A . This hallmark thus provides a convenient method for detecting the topological phase in experiments, as only a small scale of the system need be measured. The finite-size scaling of Rényi entropies S_2 and S_∞ are used to locate topological critical points, and the quantum phase diagram is obtained.

PACS numbers: 03.67.Mn, 03.65.Vf, 75.10.Pq, 64.70.Tg

I. INTRODUCTION

Without the local order parameters, the topological phases of quantum matters are beyond the Landau paradigm of phase transitions. One of the prominent example is the concept of Symmetry-Protected Topological (SPT) phase. The SPT phases are bulk-gapped quantum phases with symmetries, which have gapless or degenerate edge states as long as the symmetries are not broken.^{1,2} In one-dimensional quantum systems, the simplest theoretical model for the SPT phase could be the Affleck-Kennedy-Lieb-Tasaki (AKLT) spin-1 chain.³ The ground state of the AKLT model is exactly solvable and can be mapped into a spin-1/2 chain with the unit cell containing two spins. The nearest spins in different unit cells form the singlet, and the unit cells are projected into the spin-1 subspace. Therefore an open chain contains unpaired spins at both ends. Research on the topological properties and the edge states have been extending to other fields, such as quantum information science. Recently, the entanglement convertibility,⁴⁻⁶ a notion from quantum information science, has been used to probe the topological order. The advantage of this method is that only the information of a small scale (few sites) of the system is needed for detecting the topological order, thus greatly facilitating the experimental implementations.

The entanglement convertibility is concerned with the conversion between quantum states through the Local Operations and Classical Communication (LOCC). It is used to characterize the quantum entanglement of the states. Let us briefly review its background. Quantum entanglement describes non-separable correlations between two or more objects in a quantum state. It is a fundamental concept in quantum mechanics and has wide applications in quantum information and condensed matter.^{7,8} Considerable efforts have been made to quantify the amount of entanglement. Among them, the most investigated states are bipartite pure states, where the system, divided into two subsystems A and B , is in a pure state $|\psi_{AB}\rangle$. A well-known measure is the von Neumann entanglement entropy $S_v(\rho_A) = -\text{Tr}(\rho_A \ln \rho_A)$, where $\rho_A = \text{Tr}_B(|\psi_{AB}\rangle\langle\psi_{AB}|)$ is the reduced state of the subsystem A . This measure quantifies the entanglement of formation and entanglement of distillation.⁹ Both of them are defined in terms of the asymptotic procedure where the number of the given states and that of the Bell states are infinite in general and small errors are allowed. In particular, $S_v(\rho_A)/S_v(\rho'_A)$ gives the best ratio of M'/M if M copies of $|\psi_{AB}\rangle$ are converted into M' copies of $|\psi'_{AB}\rangle$.¹⁰ Here ρ'_A is the reduced state of the subsystem A for $|\psi'_{AB}\rangle$. A generalization of the entanglement entropy: the entanglement spectrum (ES) has been proposed.¹¹ It is defined as the eigenvalues of

the entanglement Hamiltonian H_E with $e^{-H_E} = \rho_A$. It was shown that ES can be used to classify the topological phases,^{12,13} as well as to detect the zero-energy edge modes.^{14,15}

However, the scenario is very different when only a single copy of the state is provided with the task to convert it into another single copy of the target state through LOCC. Interestingly, at the single-copy level, it is not always possible to convert a state exactly into another state with the same or lower entanglement using only LOCC. The single-copy scenario was solved for bipartite pure states through considering the Rényi entropy^{16,17}

$$S_\alpha(\rho_A) = \frac{1}{1-\alpha} \ln(\text{Tr} \rho_A^\alpha), \quad (1)$$

where $\alpha \geq 0$. The necessary and sufficient condition for the positive convertibility from the aforementioned state $|\psi_{AB}\rangle$ to $|\psi'_{AB}\rangle$ is that $S_\alpha(\rho_A) \geq S_\alpha(\rho'_A)$ for all $\alpha \geq 0$. Here a catalyst is allowed in the process of conversion. The catalyst is a bipartite state which participates in the conversion but remains intact after the conversion is finished. Whether or not the catalyst is necessary in the conversion depends on the majorization condition as follows. Suppose the eigenvalues of ρ_A are $(\omega_0, \omega_1, \omega_2, \dots) \equiv \boldsymbol{\omega}$, where $\omega_0 \geq \omega_1 \geq \omega_2 \geq \dots$ is in a non-increasing order. Similarly, the eigenvalues of ρ'_A are $(\omega'_0, \omega'_1, \omega'_2, \dots) \equiv \boldsymbol{\omega}'$. If $\sum_{j=0}^k \omega_j \leq \sum_{j=0}^k \omega'_j$ for all k , we say that $\boldsymbol{\omega}$ is majorized by $\boldsymbol{\omega}'$.¹⁸ The conversion from $|\psi_{AB}\rangle$ to $|\psi'_{AB}\rangle$ needs a catalyst if $\boldsymbol{\omega}$ is not majorized by $\boldsymbol{\omega}'$. Otherwise, the catalyst is not necessary. The Rényi entropy includes the von Neumann entanglement entropy as $\lim_{\alpha \rightarrow 1} S_\alpha(\rho_A) = S_v(\rho_A)$, and the single-copy entanglement¹⁹ as $\lim_{\alpha \rightarrow \infty} S_\alpha(\rho_A) = -\ln \omega_0$.

The Rényi entropy was used to study the properties of the ground state of the XY model in the transverse field,^{20,21} as well as the properties of the quantum state in the Kitaev chain with a quenched chemical potential.²² In both cases, the differential local convertibility (DLC) of the quantum state is related to quantum phase transitions. Here DLC refers to the convertibility between the two ground states $|\psi(g)\rangle$ and $|\psi(g+\epsilon)\rangle$, corresponding to neighboring Hamiltonian parameters g and $g+\epsilon$ (ϵ is an infinitesimal value). In particular, for the transverse Ising model as a special case,²³ the ground state is differentially convertible in the paramagnetic phase, while it can be inconvertible in the ferromagnetic phase. Specifically, DLC is related to the size of the subsystem and the correlation length of the Majorana fermions. When the subsystem size is much smaller than the correlation length of Majorana fermions, the ground state is differentially inconvertible. For the quenched Kitaev chain, the stationary quantum state is differentially inconvertible only when the subsystem size is much larger than the correlation length of Majorana fermions.²² DLC was also found to be successfully characterizing the topological order in many other models, including the cluster-Ising model, the spin-1 model,⁴ and the toric code model.^{5,6}

Recently, it was found²⁴ that DLC is not a universal indicator of the phase transitions in the spin-1/2 and spin-1 XXZ chains, but can detect the SU(2) symmetries of the system. Explicitly, for the spin-1/2 XXZ chain, the convertibility of the ground state within the antiferromagnetic Néel phase can change. In contrast, for the spin-1 XXZ model, the convertibility in the Néel phase is uniformly positive, and the transition from the Haldane to the Néel phase is detected by DLC. For both models, the local conversion changes the direction at the Heisenberg SU(2) symmetry point where the level crossing of the entanglement spectrum occurs. In this work, we study the spin-1/2 XXZ chain with bond alternation. In this model, the SU(2) symmetry point generally does not coincide with the critical point. It is interesting to investigate the behavior of DLC around the two points. We found that DLC of a large subsystem size cannot clearly distinguish the topological phase from the non-topological phase. The local convertibility is partially positive in the topological regime, and the direction of local conversion is reversed at the SU(2) symmetry point. However, for a small subsystem size, a universal property is found that the local convertibility is negative in the topological Haldane dimer phase for both cases of varying the Ising-type anisotropy Δ and the bond alternation δ . This result can be interpreted by the recombination of edge states which occurs for a small subsystem size. In the non-topological phases, the convertibility can be either negative or positive. Thus, the universally negative convertibility regarding a small subsystem size is the hallmark of the topological Haldane dimer phase. This hallmark provides a powerful tool for probing the topological order of the Haldane dimer phase. The tool facilitates the experimental implementations, as only the information of a small scale of the system is needed.

The paper is organized as follows. In Sec. II, the model of spin-1/2 XXZ chain with bond alternation is introduced and the calculation method is discussed. In Sec. III, the results on DLC are presented, where the mechanism of edge states recombination is used to interpret the inconvertibility. Finally, the conclusion is given in Sec. IV.

II. MODEL AND METHOD

Here, we will demonstrate our finding exploiting the 1d spin-1/2 alternating XXZ model. The Hamiltonians reads

$$H = \sum_{n=1}^N [1 + (-1)^n \delta] (\sigma_n^x \sigma_{n+1}^x + \sigma_n^y \sigma_{n+1}^y + \Delta \sigma_n^z \sigma_{n+1}^z). \quad (2)$$

Where $\vec{\sigma}_n$ are the Pauli matrices on the n th site of the chain with N spins. Δ is the strength of the Ising-type anisotropy which originates from the spin-orbit interaction in magnetic materials. δ is the bond alternation describing the dimerization by the spin-Peierls instability.

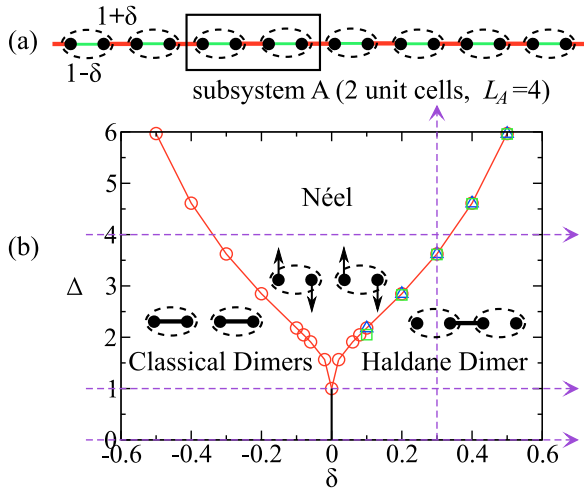


FIG. 1. (color online) (a) The bond alternating spin-1/2 XXZ model with length N . The dash ellipses define $N/2$ unit cells of the system. The coupling strength of spins in the unit cell is $1 - \delta$ (green lines), and between nearest units is $1 + \delta$ (red lines). The subsystem A contains complete unit cells. (b) The quantum phase diagram of the model is determined by using the finite-size scaling of Rényi entropies S_2 (Δ), S_∞ (\square) and the second derivative of ground state energy (\circ). The four dashed lines denote the routes that will be swept along in Sec. III.

The ground-state phase diagram is displayed in Fig. 1(b) by using the finite-size scaling of Rényi entropies and the second derivative of ground state energy. Other methods such as the von Neumann entropy and the ground-state fidelity have been used to obtain a schematic phase diagram.²⁵ Periodic boundary conditions, $\vec{\sigma}_{N+1} \rightarrow \vec{\sigma}_1$, are applied in our studies. The Hamiltonian can be experimentally realized in ion traps and optical lattices, where the bond alternation is achieved by fine tuning the intensity of the Raman laser beams.^{26–28}

The isotropic limit of the model ($\Delta = 1$) has been studied intensively.^{29–33} By choosing the unit cell (site $2n - 1$ and $2n$), as shown in Fig. 1(a), the ground state for $\delta > 1$ (ferro-antiferro alternation) is numerically shown^{30,32} to approach the spin-1 Haldane system with a finite value of the non-local string order parameter. The nearest two spins in two different unit cells tend to form a dimer (singlet) or the so-called valence bond, and the unit cells approaches to a spin-1 chain, as described by Affleck, Kennedy, Lieb, and Tasaki.³ The ground state does not break the translational symmetry by translating a unit cell. On the other hand, a small dimerization $\delta > 0$ breaks the translational symmetry (translating a lattice site) and opens a spin gap from the gapless Luttinger liquid state. The ground state becomes static dimers. Since it has been shown that there is no quantum phase transition between the dimer region ($0 < \delta \leq 1$) and the Haldane region ($\delta > 1$),³⁰ we refer to the phase as the Haldane-Dimer (HD) phase. On the other hand, for $\delta < 0$, the unit cells tend to form dimers, and the ground

state tends to be product over all unit cells. We therefore refer to the phase as the Classical Dimers (CD). Note that after choosing the unit cell, one can distinguish the HD from CD by studying the entanglement between subsystem A and B (in order to detect entanglement, the subsystem A should contain complete unit cells, *i.e.* the size of the subsystem A , L_A should be even).

In the absence of bond alternation $\delta = 0$, the model can be solved by using the Bethe ansatz,³⁴ and the ground-state phase diagram exhibits ferromagnetic ($\Delta \leq -1$), Luttinger liquid ($-1 < \Delta \leq 1$), and the Néel ($\Delta > 1$) phases.³⁵ The phase boundaries for $\delta > 0$ and $\delta < 0$ are symmetric by translation of elementary lattice spacing. In the limit of $\Delta \rightarrow \infty$, the ground state is expected to manifest the antiferromagnetic Néel order ($\uparrow\downarrow\uparrow\downarrow$) for $\delta < 1$ and double Néel order ($\uparrow\uparrow\downarrow\downarrow$) for $\delta > 1$, separated by the decoupled line $\delta = 1$. Both Néel states are nearly trivial product states.

In this paper, we focus on studying the Differential Local Convertibility (DLC), and study the edge states in the HD phase and the transitions from HD to the Néel phase, from CD to HD phase, as well as from CD to Néel phase and then to HD phase. Therefore, only the region $\Delta > 0$ and $-1 < \delta < 1$ is present. See Fig. 1(b) for the four routes (the dashed lines) that will be swept along in Sec. III.

By the Jordan-Wigner transformation, Eq. (2) can be mapping into spinless fermion chain. When $\Delta = 0$, the model is exactly solvable^{36–39} for both finite N and in the thermodynamic limit $N \rightarrow \infty$, see Appendix A for details. When $\Delta \neq 0$, we solve it numerically. We use the Density Matrix Renormalization Group (DMRG) method⁴⁰ with the recently developed parity scheme.⁴¹ The DMRG method is a powerful numerical method in quantum lattice systems, especially in one dimension. It is also suitable for studying bipartite entanglement because the bipartition and truncation are the main concepts in the DMRG algorithm. By keeping m eigenstates with largest eigenvalues of the reduced density matrix ρ_A , the bases of the subsystem are optimized and renormalized, and accurate ground state wave-function can be achieved. Unlike the quantum Monte Carlo methods which may only simulate the Rényi entropy S_α with integer $\alpha \geq 2$,^{42–44} the DMRG allows to compute S_α with a wide range of α . As we will present in this work, α is taken from 10^{-2} to 10^3 . The parity scheme of DMRG⁴¹ enables us to label the eigenstates of ρ_A by the quantum numbers S_A^z and p_A , where $S_A^z = \frac{1}{2} \sum_{n \in A} \sigma_n^z$ is the z -component of total spins and p_A is the parity (inversion) of the subsystem A . Thus the eigenvalues and eigenstates of ρ_A can be identified by (S_A^z, p_A) , which helps to better characterize the topological system.

III. DIFFERENTIAL LOCAL CONVERTIBILITY

In this section, we shall present the results of DLC and interpret them by the recombination of topological edge

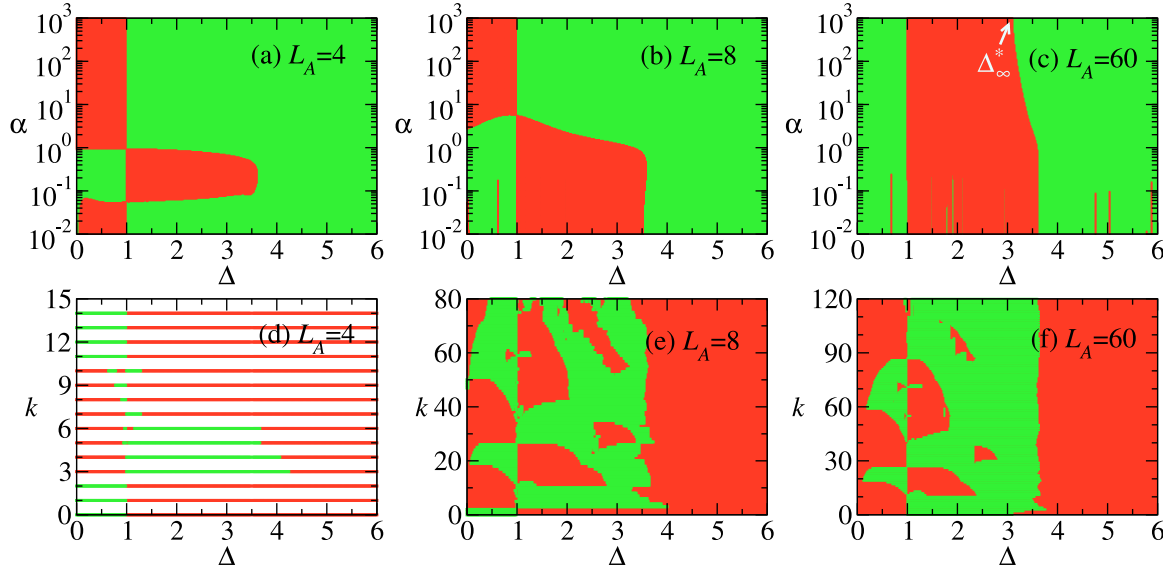


FIG. 2. (color online) (a), (b), (c) The sign of $\frac{\partial S_\alpha}{\partial \Delta}$ is plotted against Δ , where S_α is the Rényi entropy of the reduced state of subsystem A with size $L_A = 4, 8, 60$ as marked in the graphs. (d), (e), (f) The corresponding plots of majorization $M(k)$. The red color denotes that $\frac{\partial S_\alpha}{\partial \Delta} > 0$ ($M(k) > 0$) and the green color indicates that $\frac{\partial S_\alpha}{\partial \Delta} < 0$ ($M(k) < 0$). The parameters are $N = 120$, $\delta = 0.3$, $\epsilon = 5 \times 10^{-3}$. In the DMRG calculation, $m = 500$ states are kept, with the truncation error below 10^{-11} .

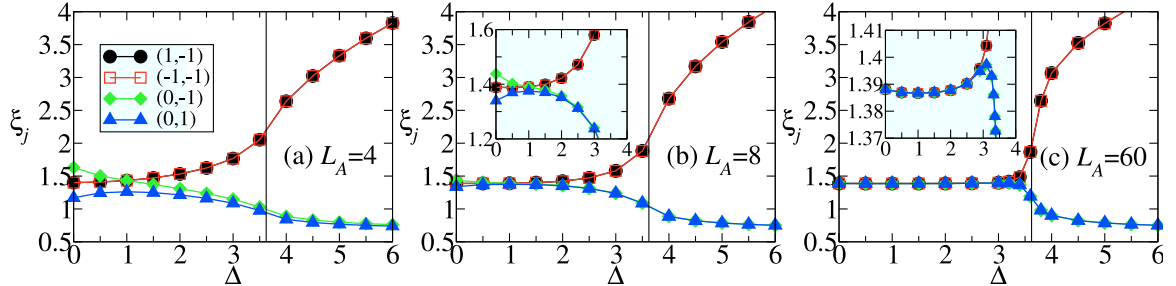


FIG. 3. (color online) (a), (b), (c) The lowest four eigenvalues of the entanglement Hamiltonian H_E , $e^{-H_E} = \rho_A$, corresponding to Fig. 2(a), (b), (c). Each line is labelled with the quantum numbers (S_A^z, p_A) , where $S_A^z = 0, \pm 1$ and $p_A = \pm 1$. See also the last paragraph of Sec. II. The insets of (b) and (c) are the zoom-in of (b) and (c). The vertical line denotes the critical point $\Delta_c \approx 3.623$ obtained by the energy derivatives.

states.

$|\psi(g + \epsilon)\rangle$ is defined as

$$M(k) = \frac{\partial}{\partial g} \sum_{j=0}^k \omega_j, \quad (3)$$

where ω_j 's are the eigenvalues of the reduced state of the subsystem. The local conversion between $|\psi(g)\rangle$ and $|\psi(g + \epsilon)\rangle$ without the aid of a catalyst is possible if the sign of $M(k)$ is uniform up to 0 (see Sec. I).

A. Sweeps along Δ

Here, we compute the DLC along the vertical sweep in Fig. 1.

Fig. 2(a), (b), (c) show the sign of $\frac{\partial S_\alpha}{\partial \Delta}$ for $0 \leq \Delta \leq 6$, $10^{-2} \leq \alpha \leq 10^3$, $\delta = 0.3$ and $N = 120$. The subsystem

DLC is concerned with the convertibility between the quantum state $|\psi(g)\rangle$ and $|\psi(g + \epsilon)\rangle$. For the Hamiltonian (2), only the ground state is considered for simplicity, and the parameter g can be either Δ or δ . When the convertibility is positive, the direction of the conversion is known from the sign of the derivative of the Rényi entropy of the reduced state: $\frac{\partial S_\alpha}{\partial g}$. If it is non-negative, then $|\psi(g)\rangle$ can be converted to $|\psi(g + \epsilon)\rangle$, while the conversion changes direction if $\frac{\partial S_\alpha}{\partial g} \leq 0$. In contrast, DLC breaks down if $\frac{\partial S_\alpha}{\partial g} \leq 0$ changes sign with α . We also considered the majorization between the above two states, from which the necessity of a catalyst can be determined and the symmetry of the reduced-state eigenvalues can be examined. The majorization between $|\psi(g)\rangle$ and

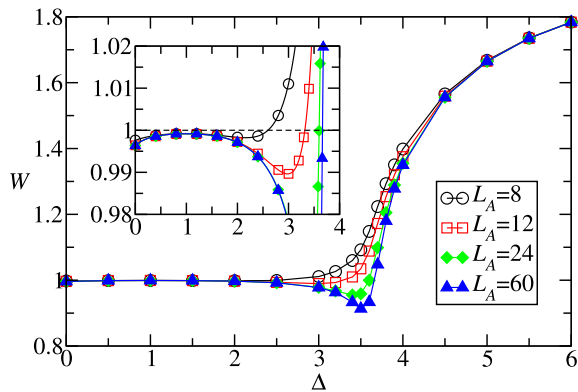


FIG. 4. (color online) The quantity $W = 4 \sum_j \omega_j^2$ is plotted against Δ for $L_A = 8, 12, 24, 60$. The inset is the zoom-in plot.

size $L_A = 4, 8, 60$. Fig. 2(d), (e), (f) show the corresponding plots of majorization. We observe that, for a generic partition, the ground state in the HD cannot be converted. Nevertheless, we observe that the convertibility tends to be restored by increasing the partitions size. This phenomenon arises since the resources encoded in larger systems increase; therefore the convertibility is enhanced. This argument applies to one of the two subsystems whose size does not exceed $N/2$, as the effect of LOCC is more restricted by this subsystem rather than the other one (similar to the Schmidt decomposition of bipartite states). In view of this property, we fix the total size of the Hamiltonian and vary the size of subsystem A.

It can be seen in Fig. 2(a), (b), (c) that for $L_A = 4, 8$, DLC breaks down when $0 \leq \Delta \lesssim 3.6$, while it is positive when $\Delta \gtrsim 3.6$. We notice that the critical point $\Delta_c \approx 3.623$ separates the topological phase ($0 \leq \Delta < \Delta_c$) from the non-topological Néel phase ($\Delta > \Delta_c$). See Fig. 2(c). It is also found that the inconvertible region in Fig. 2(c) shrinks when $L_A = N/2$ increases. We will examine it numerically in Appendix B, where it is shown that the inconvertible region disappears in the thermodynamic limit. Combining Fig. 2(c) with (f), it can be seen that the local conversion needs a catalyst in most part of the topological phase, except around $\Delta = 0$ and $\Delta = 3$. In comparison, the catalyst is not necessary in the Néel phase. The local conversion changes direction at the $SU(2)$ symmetry point $\Delta = 1$ where the majorization shows a mirror-like symmetry. Moreover, it is conceivable that in the thermodynamic limit the conversion direction changes at the critical point $\Delta_c \approx 3.623$. This is because the local conversion cannot increase the entanglement which diverges at the critical point (quantified by the von Neumann entropy, see Fig. 2(c) with $\alpha = 1$).

In the following, we shall argue that the behavior of DLC can be understood in terms of edge states formation. Fig. 3(a), (b), (c) show the lowest four eigenvalues of the entanglement Hamiltonian H_E , $e^{-H_E} = \rho_A$, for the three cases in Fig. 2. Let us consider $L_A = 60$ first. It can be seen that the four eigenvalues of the reduced

density matrix are almost degenerate in the HD phase. See also the zoom-in plot in Fig. 3(c). Moreover, it is numerically found that the whole ES is at least four-fold degenerate. This suggests that the reduced state of subsystem A is approximately

$$\rho_A \approx \begin{bmatrix} \frac{1}{2} & 0 \\ 0 & \frac{1}{2} \end{bmatrix} \otimes \rho_0 \otimes \begin{bmatrix} \frac{1}{2} & 0 \\ 0 & \frac{1}{2} \end{bmatrix}, \quad (4)$$

where ρ_0 is a $2^{L_A-2} \times 2^{L_A-2}$ matrix whose eigenvalues are equal to four times the eigenvalues of ρ_A . The two identical 2×2 matrices in Eq. (4) can be identified as the two edge states which induce the four-fold degeneracy of ES. This identification, manifesting the edge-ES correspondence,^{45–47} is supported by the two limiting cases below. (i) When $\delta = 1$, the model is simplified as the sum of disconnected two-body XXZ Hamiltonians. The ground state is a tensor product of spin singlet states. If the subsystem A is chosen in such a way that both of its boundaries cut the singlet states, its reduced state is exactly the form in Eq. (4). The state ρ_0 is a pure state composed of singlet states of the bulk, while the other two identical matrices originate from the partial trace of the singlet states at the boundaries. (ii) When $\Delta = 0$, Eq. (2) is equivalent to the Hamiltonian of non-interacting fermions, through the Jordan-Wigner transformation. See Appendix A for details. In this case, the reduced state of the subsystem can be expressed as $\rho_A = e^{-\sum_k \varepsilon_k \tilde{c}_k^\dagger \tilde{c}_k}$ up to normalization. Here \tilde{c}_k^\dagger , \tilde{c}_k are the creation, annihilation operators of the eigenmodes confined in the subsystem A with energy ε_k . When the subsystem is sufficiently long and its two boundaries cut the stronger bonds (with coupling strength $1 + \delta$, $\delta > 0$), there will be two eigenmodes which are localized about the boundaries with negligible energy, say, $\varepsilon_1 \approx \varepsilon_2 \approx 0$. As a result, the reduced state ρ_A can be written in the form of Eq. (4). For general cases ($\Delta \neq 0$ and $\delta \neq 1$), the ground state and the reduced state accordingly are complex many-body states. The four-fold ES degeneracy can be used to detect the edge states.¹²

In Fig. 4, the quantity $W = 4 \sum_j \omega_j^2$ is plotted against Δ , where $N = 120$, $L_A = 8, 12, 24, 60$ and ω_j 's are the eigenvalues of the reduced state of the subsystem A. The quantity W with a large subsystem size basically shows the purity of the bulk ρ_0 : $\text{tr}(\rho_0^2) \approx 4\text{tr}(\rho_A^2) = 4 \sum_j \omega_j^2$. It reflects the correlation between the bulk sites and the two edges, as interpreted below. Fig. 4 shows that the purity of the bulk state increases with Δ to reach a maximum at $\Delta = 1$, and then it starts to decrease. This behavior indicates that the bulk sites become less correlated with the two edges when Δ increases to approach 1, while they do the opposite when $\Delta > 1$. This point can be understood by considering the special case $\delta = 1$ where the bulk state is a pure state composed of singlet states so that the bulk sites are completely uncorrelated with the edges. Therefore, the lowest four eigenvalues of H_E have a local minimum at $\Delta = 1$, where they are closest to $-\ln 0.25 \approx 1.386$. See the inset of Fig. 3(c). The bifurcation occurs when $\Delta \gtrsim 3.1$, showing that the four-

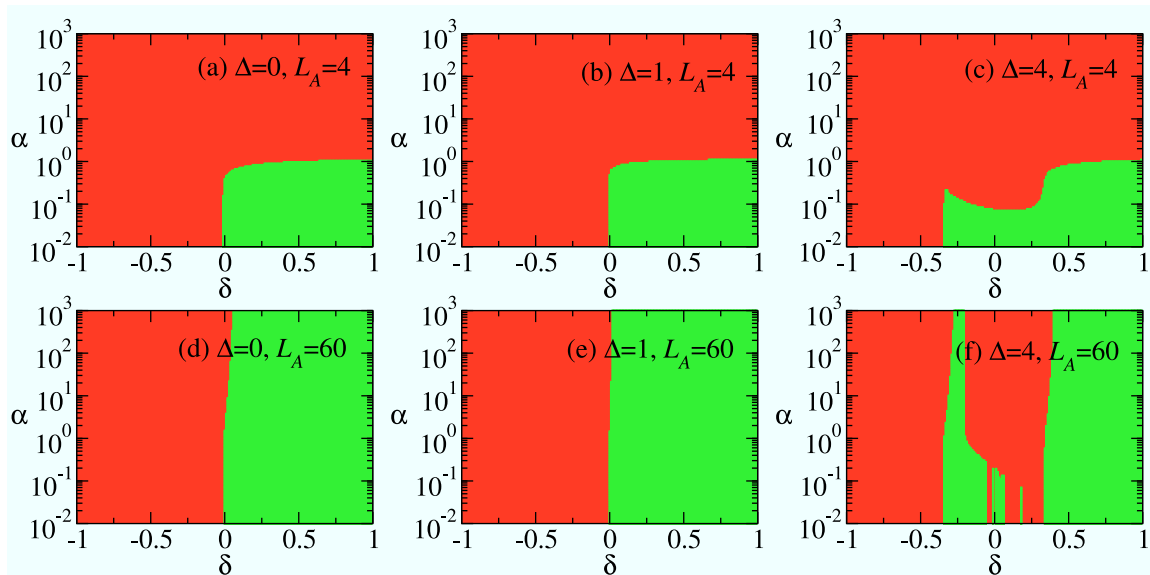


FIG. 5. (color online) The sign of $\frac{\partial S_\alpha}{\partial \Delta}$ are plotted against δ , where S_α is the Rényi entropy of the reduced state of subsystem A. (a), (b), (c) The subsystem size $L_A = 4$, $\Delta = 0, 1, 4$. (d), (e), (f) $L_A = 60$, $\Delta = 0, 1, 4$. The total size is $N = 120$ ($N \rightarrow \infty$ for $\Delta = 0$).

fold ES degeneracy is partially lifted. As a consequence, Eq. (4) is no longer applicable. It's conceivable that the edge states start recombining, resulting in the splitting of the lowest four eigenvalues of H_E . In particular, $\xi_0 \equiv -\ln \omega_0$ will decrease with Δ .

The above analysis is consistent with DLC in Fig. 2(c). Since $\lim_{\alpha \rightarrow \infty} S_\alpha(\rho_A) = -\ln \omega_0$, the sign of $\frac{\partial S_\alpha}{\partial \Delta}$ for large α in Fig. 2 can be derived from Fig. 3(f). In addition, when $\alpha \rightarrow 1$, the Rényi entropy reduces to the von Neumann entropy which has been shown to diverge at critical points.^{48–50} This result was verified in the spin-1/2 XXZ chain with bond alternation.²⁵

Next, we consider $L_A = 4, 8$. Comparing Fig. 2(a), (b) with (c), we find that the inconvertible region in Fig. 2(c) increases when the subsystem size decreases. Namely, the ground state changes from convertible to non-convertible for values of Δ that are smaller than Δ_c . This indicates that the edge states start recombining at smaller Δ when L_A decreases. Note that $\Delta = 1$ no longer separates the positive and negative DLC regions: all the regions in HD phase are locally inconvertible due to the recombination of edge states for small L_A .

In the final part of the present subsection, we shall give a physical interpretation for Fig. 3(a), (b). Roughly speaking, the term $\sum_n \Delta \sigma_n^z \sigma_{n+1}^z$ tends to anti-parallel the z components of neighboring spins, which has an effect that the z components of spins of the two edges of subsystem A are also anti-parallel. Thus, the probability ω_j of the eigenstates with quantum number $(S_A^z, p_A) = (0, -1)$ of ρ_A increases with Δ . These eigenstates are the anti-parallel component of the triplet states with $p_A = -1$. Based on this picture, the change of ES ($\xi_j = -\ln \omega_j$) when Δ is varied, as shown in Fig. 3(a),

(b), can be understood. Both the Schmidt states with quantum number $(0, -1)$ and those with $(0, 1)$ have anti-parallel z components of spins for the two edges. The reason why the term $\sum_n \Delta \sigma_n^z \sigma_{n+1}^z$ prefers the former to the latter when $0 \leq \Delta \leq 1$ is related to the ES level crossing at the SU(2) symmetry point $\Delta = 1$. We notice that due to the level crossing, the sign of the derivative of Rényi entropy flips at $\Delta = 1$ for all α . This means that the ES of the singlet state with quantum number $(0, 1)$ has an extreme point at $\Delta = 1$ and around it a mirror-like symmetry is present.²⁴

The reduced state of the special case $\Delta = 0$ is shown in Eq. (A7). It can be seen in Fig. 3(a), (b) that the ES splitting becomes smaller when Δ increases from 0 to 1, and then it becomes larger when Δ increases further. These results indicate that there is a minimum recombination of the edge states at $\Delta = 1$. Beyond the critical point, the edge states disappear and the system goes to the Néel phase. In this phase the ground state is convertible.

B. Sweeps along δ

Fig. 5 shows the sign of $\frac{\partial S_\alpha}{\partial \Delta}$ for $-1 \leq \delta \leq 1$, $10^{-1} \leq \alpha \leq 10^3$, $\Delta = 0, 1, 4$ and $L_A = 4, 60$. The case $\Delta = 0$ is calculated by using the correlation matrix formalism in Appendix A with $N \rightarrow \infty$. For $\Delta = 1, 4$, DMRG is used and $N = 120$. The topological regime is $0 < \delta \leq 1$ for $\Delta = 0, 1$, and $0.35 \lesssim \delta \leq 1$ for $\Delta = 4$.

It can be seen in Fig. 5 that in the topological phase, DLC of small sizes is negative, but DLC of a large size is partially positive. These results can be interpreted by

the recombination of edge states. This is analogous to the previous section. Moreover, the inconvertible region in the topological phase shrinks when L_A increases, and it will disappear in the thermodynamic limit (this will be discussed in Appendix B). This phenomenon also happens in the previous section when Δ is varied. However, the local conversion in most part of the convertible topological phase there needs a catalyst, which is not needed here (the majorization is not shown for brevity). This means that the catalytic conversion may not be universal for characterizing the topological phase in the thermodynamic limit.

As for the non-topological phases, DLC can be either negative or positive, which differs considerably from Fig. 2. In particular, DLC is totally negative in the Néel phase in Fig. 5(c), and it is partially negative in Fig. 5(f). This provides an evidence of the non-universality of convertibility for detecting the topological phase,²⁴ in addition to the partially positive DLC of a large size mentioned in the previous paragraph. The behaviour of the entanglement spectrum for $-0.35 < \delta < 0.35$ can be explained as follows. Since the Rényi entropies diverge at the two critical points $\delta \approx \pm 0.35$ for infinite L_A , there must be two maxima respectively around the two points for large L_A . Apparently, a minimum between the two maxima is present for every α , as can be seen in Fig. 5(f). The value of δ corresponding to this minimum in general varies with α (unless some additional symmetry is present in the subsystem A, like the SU(2) at $\Delta = 1$ in Fig. 2(c), but it does not seem to exist here). As a result, negative DLC emerges in the Néel phase.

IV. CONCLUSION

By using the DMRG with parity quantum numbers⁴¹ and the correlation function matrix formalism,^{38,39} we have investigated the entanglement convertibility in the one-dimensional spin-1/2 XXZ model with bond alternation. It is found that the subsystem-size effect is crucial for looking for the universal properties of DLC. For a small subsystem size L_A , the convertibility is universally negative in the topological Haldane dimer phase. The negative convertibility is attributed to the recombination of edge states which occurs for small L_A . When L_A increases, the edge states only recombines in the region closer to the phase boundary, rendering the convertibility partially negative. In the non-topological phases, the convertibility can be either positive or negative. For instance, it is positive when Δ is varied and $0 < \delta < 1$ is fixed. In comparison, negative convertibility emerges in the Néel phase when δ is varied and $\Delta > 1$ is fixed. Therefore, the universally negative convertibility regarding small L_A is the hallmark of the topological Haldane dimer phase. This hallmark provides a powerful tool for probing the topological order of the Haldane dimer phase. The tool facilitates the experimental implementations,⁵¹ as only a small scale of the system need be measured. The

finite-size scaling of the maximum of Rényi entropies S_α with $\alpha \rightarrow \infty$ and $\alpha = 2$ are used to locate the critical point. It is compared with the finite-size scaling of second derivatives of ground state energy density and they agree well. The precise ground-state phase diagram is determined.

In the thermodynamic limit, the local conversion along Δ needs a catalyst in most part of the topological phase, whereas it is unnecessary when δ is varied. The contrast indicates a differing computational power in terms of the need of a catalyst in quantum simulation via local operations and classical communication. The fact that this happens within the same topological phase might pose a question on whether the computational power of the topological phase is universally more efficient than the classical algorithms. This is interesting for future study.

ACKNOWLEDGMENTS

We are grateful to MOST in Taiwan for the financial supports via NSC-102-2112-M-005-001-MY3(Y.C.T. & M.C.C.) and MOST-104-2811-M-005-012(L.D.). Y.C.T. is grateful to Hsing Tian Kong Culture & Education Development Foundation for the scholarship. Y.C.T. is grateful to Prof. Guang-Yin Chen and Prof. Wen-Min Huang for providing computing facilities. L.C.K. acknowledges support from the National Research Foundation & Ministry of Education, Singapore.

Appendix A: Dimerized chain of non-interacting spinless fermions

When $\Delta = 0$, the Hamiltonian in Eq. (2) can be mapped to the dimerized chain of non-interacting spinless fermions³⁶ through the Jordan-Wigner transformation, and the entanglement spectrum can be computed using the correlation function matrix (CFM) formalism.^{38,39}

The Jordan-Wigner transformation is

$$c_j = \sigma_j \prod_{k=1}^{j-1} (-\sigma_k^z), \quad (\text{A1})$$

where $\sigma_j = (\sigma_j^x - i\sigma_j^y)/2$. Substituting Eq. (A1) into Eq. (2), we have

$$\begin{aligned} H = & -2 \sum_{n=1}^{N-1} [1 + (-1)^n \delta] (c_n c_{n+1}^\dagger + c_{n+1} c_n^\dagger) \\ & + 2[1 + (-1)^N \delta] (c_N c_1^\dagger + c_1 c_N^\dagger) \prod_{j=1}^N (1 - 2c_j^\dagger c_j). \end{aligned} \quad (\text{A2})$$

Assume N is an even number and $M = N/2$. Since the number operator $\sum_j c_j^\dagger c_j$ commutes with the Hamiltonian, the eigenstates of the Hamiltonian can be solved

in the subspace of conserved number of particles. In particular, it will be shown later that the ground state is non-degenerate and contains M particles (*i.e.* half-filled) when $\delta \neq 0$. In this case, the operator $\prod_{j=1}^N (1 - 2c_j^\dagger c_j)$ in Eq. (A2) is equal to $(-1)^M$. Thus, we have a free fermion chain with periodic boundary conditions (PBC) when M is odd, while the boundary condition is anti-periodic when M is even.

Perform the Fourier transformation

$$c_{2j-1} = \frac{1}{\sqrt{M}} \sum_{k=1}^M a_k e^{i \frac{p_k \pi}{M} j}, \quad (\text{A3})$$

$$c_{2j} = \frac{1}{\sqrt{M}} \sum_{k=1}^M b_k e^{i \frac{p_k \pi}{M} j}, \quad (\text{A4})$$

where p_k depends on M : when M is odd, $p_k = 2k$, otherwise $p_k = 2k + 1$. The choice of p_k is to ensure that the Fourier transformation works for both PBC and anti-PBC fermion chains. The Hamiltonian is transformed into

$$H = \sum_{k=1}^M \begin{bmatrix} a_k^\dagger & b_k^\dagger \end{bmatrix} [\mathbf{R}(k) \cdot \boldsymbol{\sigma}] \begin{bmatrix} a_k \\ b_k \end{bmatrix}, \quad (\text{A5})$$

where $\mathbf{R}(k) = (R_x(k), R_y(k), R_z(k))$, $R_x(k) = 2(1 - \delta) + 2(1 + \delta) \cos \frac{p_k \pi}{M}$, $R_y(k) = 2(1 + \delta) \sin \frac{p_k \pi}{M}$, $R_z(k) = 0$, and $\boldsymbol{\sigma} = (\sigma_x, \sigma_y, \sigma_z)$ is the vector of Pauli matrices. The length of $\mathbf{R}(k)$ is $R(k) = 4\sqrt{\cos^2 \frac{p_k \pi}{2M} + \delta^2 \sin^2 \frac{p_k \pi}{2M}}$. The Hamiltonian has two bands with energy $\pm R(k)$. When $\delta \neq 0$, $R(k)$ is nonzero for all k and the two bands are gapped. The ground state corresponds to the occupied negative-energy band (half-filled) and it is non-degenerate. When $\delta = 0$, the Hamiltonian is gapless, since the two bands touch when $M \rightarrow \infty$ ($R(k) \rightarrow 0$ for $p_k/M \rightarrow 1$).

The topological properties of the chain can be characterized by the Berry phase³⁷ $\gamma \equiv \int_0^{2\pi} dk \langle \phi | i \partial_k | \phi \rangle$, where $|\phi\rangle$ is the eigenvector of $\mathbf{R}(k) \cdot \boldsymbol{\sigma}$ with the eigenvalue $-R(k)$. It can be shown that $\gamma = n_w \pi$ modulo 2π , where $n_w \equiv \frac{1}{2\pi} \int_0^{2\pi} \frac{d\theta}{dk} dk = [1 + \text{sign}(\delta)]/2$. Here θ is the polar angle: $\tan(\theta) = R_y(k)/R_x(k)$. The quantity n_w is the winding number describing the total number of times that $\mathbf{R}(k)$ surrounds the origin of the $(R_x(k), R_y(k))$ parametric space when k changes from 0 to 2π . A nonzero n_w (*i.e.* $\delta > 0$) defines the topological phase, where the chain with open-boundary conditions supports two edge modes. For PBC, the reduced state of subsystem has two edge modes when two stronger bonds are cut off. This can be derived by the CFM below.

The CFM is defined as $C_{m,n} = \langle \phi_0 | \mathbf{c}_m \mathbf{c}_n^\dagger | \phi_0 \rangle$, where $|\phi_0\rangle$ is the ground state and $\mathbf{c}_m = [c_{2m-1} \ c_{2m}]^T$. It can be verified that $C_{m,n} = \frac{1}{M} \sum_k e^{i \frac{p_k \pi}{M} (m-n)} G(k)$, where $G(k)$ is the CFM in momentum space:³⁹

$$G(k) = \frac{1}{2} [I_{2 \times 2} + \hat{\mathbf{R}}(k) \cdot \boldsymbol{\sigma}], \quad (\text{A6})$$

where $\hat{\mathbf{R}}(k) = \mathbf{R}(k)/R(k)$ is a unit vector. The reduced state of subsystem A is $\rho_A = \frac{1}{Z} e^{-\sum_l \varepsilon_l \tilde{c}_l^\dagger \tilde{c}_l}$, where $Z = \text{tr}(e^{-\sum_l \varepsilon_l \tilde{c}_l^\dagger \tilde{c}_l})$ is the normalization constant, $\varepsilon_l = \ln \frac{q_l}{1-q_l}$, $\tilde{c}_l = \sum U_{lm} c_m$, and U is the unitary matrix that diagonalizes the CFM with eigenvalues q_l (*i.e.* $U[C_{m,n}]U^\dagger$ is a diagonal matrix).

When the subsystem is defined by cutting off two stronger bonds, there will be two zero-energy edge modes, say $q_1 \approx q_2 \approx \frac{1}{2}$. We have

$$\begin{aligned} \rho_A &= \rho_0 \otimes \frac{1}{Z_1} e^{-\varepsilon_1 (\tilde{c}_1^\dagger \tilde{c}_1 - \tilde{c}_2^\dagger \tilde{c}_2)}, \\ &= \begin{bmatrix} \frac{1}{2} - \lambda & 0 \\ 0 & \frac{1}{2} + \lambda \end{bmatrix} \otimes \rho_0 \otimes \begin{bmatrix} \frac{1}{2} + \lambda & 0 \\ 0 & \frac{1}{2} - \lambda \end{bmatrix}, \end{aligned} \quad (\text{A7})$$

where ρ_0 is the reduced state of all the eigen-modes excluding the edge modes, $Z_1 = \text{tr}(e^{-\varepsilon_1 (\tilde{c}_1^\dagger \tilde{c}_1 - \tilde{c}_2^\dagger \tilde{c}_2)})$, ε_1 is positive and equals $\ln \frac{q_1}{1-q_1} \approx 0$, $\lambda = q_1 - \frac{1}{2}$, $\tilde{c}_1^\dagger = \frac{1}{\sqrt{2}} (\tilde{c}_L^\dagger - \tilde{c}_R^\dagger)$, $\tilde{c}_2^\dagger = \frac{1}{\sqrt{2}} (\tilde{c}_L^\dagger + \tilde{c}_R^\dagger)$. Here, $\tilde{c}_L^\dagger, \tilde{c}_R^\dagger$ are the creation operators of the left and right edge modes. The wave function for the edge modes can be derived from the eigenvectors of ρ_A (corresponding to the eigenvalues $q_{1,2}$). The form of $\tilde{c}_{1,2}^\dagger$ is consistent with the requirement that ρ_A commutes with the inversion symmetry operator within subsystem A. Note that Eq. (A7) is a special case of Eq. (4). Also, the two degenerate entanglement spectra at $\Delta = 0$ in Fig. 3(a) can be understood by inspecting the matrix elements of the two edge states in Eq. (A7).

The Rényi entropy of ρ_A when $\Delta = 0$ is simplified as

$$S_\alpha(\rho_A) = \frac{1}{1-\alpha} \sum_{j=1}^{L_A} \ln[q_j^\alpha + (1-q_j)^\alpha]. \quad (\text{A8})$$

Appendix B: Phase diagram

In this section, with the finite-size scaling, we study the topological HD phase boundaries. We have shown in the previous section that the topological states are not convertible for a small subsystem $L_A = 4$. However, since the non-topological phase there may also present negative convertibility, one can not in general detect the topological transitions by examining the boundary of convertibility. We therefore look for other quantities in the case of half-half bipartition, $L_A = N/2$, and performing extrapolation to the thermodynamic limit $N \rightarrow \infty$. Recent studies⁵² have shown the non-universality of entanglement spectrum and Rényi entropies S_α in the sense that they may exhibit excessive singular changes within the same physical phase. However, S_α can still be used to locate the critical point, since S_α for all α are also singular⁵³ at the critical point. We concentrate on two special cases of S_α : $\alpha \rightarrow \infty$ and $\alpha = 2$, as they are closely related to DLC. Other values of α can also be considered, which are omitted here.

The sign-changed point Δ_∞^* of DLC for infinite α , as pointed out in the Fig. 2(c). This point indicates the

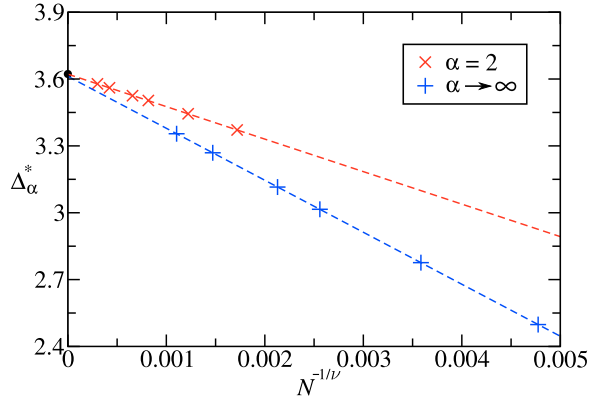


FIG. 6. (color online) Extrapolation of critical points from the Rényi entropies with $\alpha = 2$ and $\alpha \rightarrow \infty$ for the sweeps along Δ while fixing $\delta = 0.3$. The critical point $\Delta_c \approx 3.622$ and 3.612 for $\alpha = 2$ and $\alpha \rightarrow \infty$, with the exponents $\nu \approx 0.653$ and 0.778 , respectively. The black point denotes the critical value of $\Delta_c \approx 3.623$ obtained from the 2nd derivatives of ground state energy.

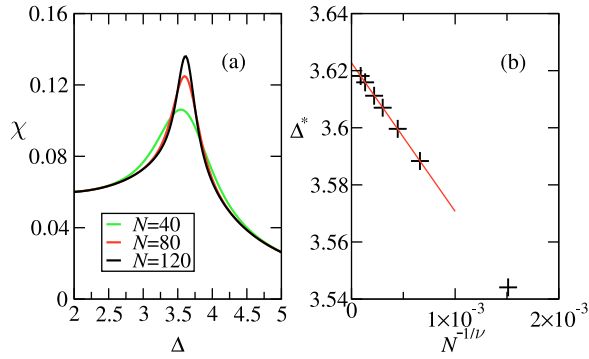


FIG. 7. (color online) (a) The 2nd derivatives of ground state energy density $\chi = -\partial^2 e_0 / \partial \Delta^2$ as a function of Δ for fixed $\delta = 0.3$ with different sizes N . (b) The extrapolation of the pseudo-critical points Δ^* . It is obtained $\Delta_c \approx 3.623$ with the exponent $\nu \approx 0.568$.

beginning of the recombination of edge states. We refer to this point as the pseudo-critical point for a finite N . When $N \rightarrow \infty$, it converges to the infinite system's critical point. We numerically determine the pseudo-critical point Δ_∞^* such that $\partial_\Delta S_\infty = \partial_\Delta \xi_0 = 0$, where ξ_0 is the lowest eigenvalue of the entanglement Hamiltonian. When the system size N increases, the shift of this point represents the shrink of the region of negative convertibility. As shown in Fig. 6, Δ_∞^* approaches the critical point $\Delta_c \approx 3.612$ in the thermodynamics limit $N \rightarrow \infty$. In fact, the Rényi entropies exhibit logarithmic divergence: $S_\alpha \propto \ln L_A$ in an infinite gapless one-dimensional model.⁵³ Thus, the extreme point of Rényi entropies must converge to the same critical point when $N \rightarrow \infty$. Now we have more confidence to say that, for fixed δ and varying the anisotropy parameter Δ with half-half bipartition, both the HD phase and Néel phase have positive convertibilities in the thermodynamic limit.

We now consider the Rényi entropy with $\alpha = 2$. There are three advantages. (i) It reflects the purity of ρ_A as $S_2 = -\ln \text{tr}(\rho_A^2)$. It is also related to the quantity W in Fig. 4 and thus the purity of the bulk state ρ_0 when Eq. (4) is valid: $S_2 = -\ln \frac{W}{4} \approx -\ln \frac{\text{tr}(\rho_0^2)}{4}$. (ii) S_2 can be measured directly in experiments without reconstructing the eigenvalues of ρ_A .^{51,54,55} (iii) In the quantum Monte Carlo methods, for $\alpha = 1$, the von Neumann entropy S_v is difficult to simulate. Rényi entropies with integer $\alpha \geq 2$, especially S_2 is easier to be simulated.⁴²⁻⁴⁴ We numerically determine the pseudo-critical point Δ_2^* by locating the maximum of S_2 , which is also the minimum of W in Fig. 4. As shown in Fig. 6, for $\delta = 0.3$ the critical point $\Delta_c \approx 3.622$ is obtained precisely.

However, when very small value of $\delta \approx 0^+$ is fixed, the HD phase are close to the critical Luttinger liquid for the region $\Delta \lesssim 1$, and the correlation lengths are large. The typical DLC, as in Fig. 2(c), should only appear when the subsystem size is much larger than the correlation length. This makes numerical difficulty for finding the proper pseudo-critical point Δ_α^* . Therefore modifying the scanning route may also be considered, *i.e.* fixing Δ and varying δ . The precise ground-state phase diagram for the bond alternating XXZ model, shown in the Fig. 1(b), is determined by the above two methods and the scaling of the second derivatives of ground state energy density which is discussed below.

According to Ehrenfest's classification of phase transitions, the n th order quantum phase transition presents non-analyticity of the n th derivatives of ground state energy density at the critical point. It has been firstly shown that the 2nd derivative of ground state energy diverges at the 2nd order quantum critical point, but it remains a finite value for the 3rd and 5th order quantum phase transitions.⁵⁶ We report the results of energy derivatives for finding the critical points of the bond-alternating XXZ model Eq. (2). The ground state energy per site $e_0 = -\frac{1}{N} \sum_k R(k)$ for $\Delta = 0$ can be exactly obtained from Appendix A. In the thermodynamic limit $N \rightarrow \infty$, $e_0 = -\frac{4}{\pi} I(1 - \delta^2)$, where $I(x) = \int_0^{\frac{\pi}{2}} \sqrt{1 - x \sin^2 \theta} d\theta$ is the complete elliptic integral of the second kind. When $\delta = 0$, we have $e_0 = -\frac{\pi}{4}$, $\partial_\delta e_0 = 0$, and $\partial_\delta^2 e_0 \rightarrow -\infty$. Therefore, for the case $\Delta = 0$, the quantum phase transition at $\delta = 0$ belongs to second-order.

When $\Delta \neq 0$, by using DMRG, the 2nd derivative is calculated by the finite difference formula

$$\frac{\partial^2 e_0(g)}{\partial g^2} \approx \frac{e_0(g - \epsilon) - 2e_0(g) + e_0(g + \epsilon)}{\epsilon^2}. \quad (\text{B1})$$

Where $e_0(g)$ is the ground state energy per site, g is the parameter of the Hamiltonian Eq. (2), and ϵ is taken to be 5×10^{-3} .

In absence of bond alternation, $\delta = 0$, it is known the system undergoes a Berezinskii-Kosterlitz-Thouless (BKT) quantum phase transition at the critical point $\Delta_c = 1$.³⁵ The BKT quantum phase transition is an

infinite-order transition, and the n th derivative of energy diverges only if $n \rightarrow \infty$. However, the order of the transitions could be different and depend on the path in the phase diagram. It was first shown by Cross and Fisher²⁹ that the ground energy density of bond-alternating Heisenberg is in proportion to $\delta^{4/3}$, and the 2nd derivatives of energy density $\partial_\delta^2 e_0 \propto \delta^{-2/3}$. Thus the 2nd derivatives of energy density diverges and indicates a second order quantum phase transition at $\delta = 0$. On the

other hand, for varying Δ and fixed $\delta = 0.3$, as shown in Fig. 7(a) and (b), the 2nd derivative of energy density diverges at the critical point $\Delta_c \approx 3.623$ in the thermodynamic limit $N \rightarrow \infty$. The values of the critical points obtained by the energy derivatives thus provide references for the values determined by the Rényi entropies S_2 and S_∞ . The precise phase diagram determined by the energy derivatives and the Rényi entropies is shown in the Fig. 1(b).

-
- ¹ Xie Chen, Zheng-Cheng Gu, Zheng-Xin Liu, and Xiao-Gang Wen, “Symmetry-protected topological orders in interacting bosonic systems,” *Science* **338**, 1604–1606 (2012).
 - ² Xie Chen, Zheng-Cheng Gu, Zheng-Xin Liu, and Xiao-Gang Wen, “Symmetry protected topological orders and the group cohomology of their symmetry group,” *Phys. Rev. B* **87**, 155114 (2013).
 - ³ Ian Affleck, Tom Kennedy, Elliott H. Lieb, and Hal Tasaki, “Rigorous results on valence-bond ground states in antiferromagnets,” *Phys. Rev. Lett.* **59**, 799–802 (1987).
 - ⁴ Jian Cui, Luigi Amico, Heng Fan, Mile Gu, Alioscia Hama, and Vlatko Vedral, “Local characterization of one-dimensional topologically ordered states,” *Phys. Rev. B* **88**, 125117 (2013).
 - ⁵ Alioscia Hama, Lukasz Cincio, Siddhartha Santra, Paolo Zanardi, and Luigi Amico, “Local response of topological order to an external perturbation,” *Phys. Rev. Lett.* **110**, 210602 (2013).
 - ⁶ Siddhartha Santra, Alioscia Hama, Lukasz Cincio, Yigit Subasi, Paolo Zanardi, and Luigi Amico, “Local convertibility of the ground state of the perturbed toric code,” *Phys. Rev. B* **90**, 245128 (2014).
 - ⁷ Luigi Amico, Rosario Fazio, Andreas Osterloh, and Vlatko Vedral, “Entanglement in many-body systems,” *Rev. Mod. Phys.* **80**, 517–576 (2008).
 - ⁸ Ryszard Horodecki, Paweł Horodecki, Michał Horodecki, and Karol Horodecki, “Quantum entanglement,” *Rev. Mod. Phys.* **81**, 865–942 (2009).
 - ⁹ Michael A. Nielsen and Isaac L. Chuang, *Quantum Computation and Quantum information* (Cambridge University Press, 2000).
 - ¹⁰ Charles H. Bennett, Herbert J. Bernstein, Sandu Popescu, and Benjamin Schumacher, “Concentrating partial entanglement by local operations,” *Phys. Rev. A* **53**, 2046–2052 (1996).
 - ¹¹ Hui Li and F. D. M. Haldane, “Entanglement spectrum as a generalization of entanglement entropy: Identification of topological order in non-abelian fractional quantum hall effect states,” *Phys. Rev. Lett.* **101**, 010504 (2008).
 - ¹² Frank Pollmann, Ari M. Turner, Erez Berg, and Masaki Oshikawa, “Entanglement spectrum of a topological phase in one dimension,” *Phys. Rev. B* **81**, 064439 (2010).
 - ¹³ Johannes Motruk, Erez Berg, Ari M. Turner, and Frank Pollmann, “Topological phases in gapped edges of fractionalized systems,” *Phys. Rev. B* **88**, 085115 (2013).
 - ¹⁴ Lukasz Fidkowski, “Entanglement spectrum of topological insulators and superconductors,” *Phys. Rev. Lett.* **104**, 130502 (2010).
 - ¹⁵ Ming-Chiang Chung, Yi-Hao Jhu, Pochung Chen, and Sungkit Yip, “Edge states, entanglement entropy spectra and critical hopping couplings of anisotropic honeycomb lattices,” *EPL* **95**, 27003 (2011).
 - ¹⁶ S. Turgut, “Catalytic transformations for bipartite pure states,” *J. Phys. A: Math. Theor.* **40**, 12185 (2007).
 - ¹⁷ M. Klimesh, “Inequalities that collectively completely...” (2007), arXiv: 0709.3680.
 - ¹⁸ M. A. Nielsen, “Conditions for a class of entanglement transformations,” *Phys. Rev. Lett.* **83**, 436–439 (1999).
 - ¹⁹ Román Orús, *Entanglement, quantum phase transitions and quantum algorithms*, Ph.D. thesis, University of Barcelona (2006), arXiv:quant-ph/0608013.
 - ²⁰ Jian Cui, Mile Gu, Leong-Chuan Kwek, M. F. Santos, Heng Fan, and Vlatko Vedral, “Quantum phases with differing computational power,” *Nat. Commun.* **3**, 812 (2012).
 - ²¹ Si-Yuan Liu, Quan Quan, Jin-Jun Chen, Yu-Ran Zhang, Wen-Li Yang, and Heng Fan, “Phase diagram of quantum critical system via local...” (2015), arXiv: 1510.07115.
 - ²² Li Dai and Ming-Chiang Chung, “Breakdown of local convertibility through Majorana modes in a quantum quench,” *Phys. Rev. A* **91**, 062319 (2015).
 - ²³ Fabio Franchini, Jian Cui, Luigi Amico, Heng Fan, Mile Gu, Vladimir Korepin, Leong-Chuan Kwek, and Vlatko Vedral, “Local convertibility and the quantum simulation of edge states in many-body systems,” *Phys. Rev. X* **4**, 041028 (2014).
 - ²⁴ Helena Bragança, Eduardo Mascarenhas, G. I. Luiz, C. Duarte, R. G. Pereira, M. F. Santos, and M. C. O. Aguiar, “Nonuniversality of entanglement convertibility,” *Phys. Rev. B* **89**, 235132 (2014).
 - ²⁵ Ling Qiang, Guang-Hua Liu, and Guang-Shan Tian, “Effects of bond alternation on the ground-state phase diagram of one-dimensional xxz model,” *Commun. Theor. Phys.* **60**, 240 (2013).
 - ²⁶ L.-M. Duan, E. Demler, and M. D. Lukin, “Controlling spin exchange interactions of ultracold atoms in optical lattices,” *Phys. Rev. Lett.* **91**, 090402 (2003).
 - ²⁷ Yu-Ao Chen, Sylvain Nascimbène, Monika Aidelsburger, Marcos Atala, Stefan Trotzky, and Immanuel Bloch, “Controlling correlated tunneling and superexchange interactions with ac-driven optical lattices,” *Phys. Rev. Lett.* **107**, 210405 (2011).
 - ²⁸ S Korenblit, D Kafri, W C Campbell, R Islam, E E Edwards, Z-X Gong, G-D Lin, L-M Duan, J Kim, K Kim, and C Monroe, “Quantum simulation of spin models on an arbitrary lattice with trapped ions,” *New J. Phys.* **14**, 095024 (2012).
 - ²⁹ M. C. Cross and Daniel S. Fisher, “A new theory of the spin-peierls transition with special relevance to the experiments on TTFCuBDT,” *Phys. Rev. B* **19**, 402–419 (1979).

- ³⁰ Kazuo Hida, “Crossover between the Haldane-gap phase and the dimer phase in the spin-1/2 alternating Heisenberg chain,” *Phys. Rev. B* **45**, 2207–2212 (1992).
- ³¹ Masaaki Nakamura and Synge Todo, “Order parameter to characterize valence-bond-solid states in quantum spin chains,” *Phys. Rev. Lett.* **89**, 077204 (2002).
- ³² Hsiang-Hsuan Hung and Chang-De Gong, “Numerical evidence of a spin-1/2 chain approaching a spin-1 chain,” *Phys. Rev. B* **71**, 054413 (2005).
- ³³ Liu Guang-Hua and Tian Guang-Shan, “Matrix product state, quantum entanglement, and criticality in the one-dimensional dimerized antiferromagnetic Heisenberg model,” *Comm. Theo. Phys.* **58**, 285 (2012).
- ³⁴ C. N. Yang and C. P. Yang, “One-dimensional chain of anisotropic spin-spin interactions. I. proof of Bethe’s hypothesis for ground state in a finite system,” *Phys. Rev.* **150**, 321–327 (1966).
- ³⁵ Thierry Giamarchi, *Quantum physics in one dimension* (Oxford University Press, 2003).
- ³⁶ W. P. Su, J. R. Schrieffer, and A. J. Heeger, “Solitons in polyacetylene,” *Phys. Rev. Lett.* **42**, 1698–1701 (1979).
- ³⁷ Shun-Qing Shen, *Topological Insulators: Dirac Equation in Condensed Matters*, Vol. 174 (Springer Science & Business Media, 2013).
- ³⁸ Ingo Peschel, “Calculation of reduced density matrices from correlation functions,” *J. Phys. A: Math. Gen.* **36**, L205 (2003).
- ³⁹ Ming-Chiang Chung, Yi-Hao Jhu, Pochung Chen, and Chung-Yu Mou, “Quench dynamics of topological maximally entangled states,” *J. Phys.: Condens. Matter* **25**, 285601 (2013).
- ⁴⁰ Steven R. White, “Density matrix formulation for quantum renormalization groups,” *Phys. Rev. Lett.* **69**, 2863–2866 (1992).
- ⁴¹ Yu-Chin Tzeng, “Parity quantum numbers in the density matrix renormalization group,” *Phys. Rev. B* **86**, 024403 (2012).
- ⁴² Chia-Min Chung, Lars Bonnes, Pochung Chen, and Andreas M. Läuchli, “Entanglement spectroscopy using quantum monte carlo,” *Phys. Rev. B* **89**, 195147 (2014).
- ⁴³ C. M. Herdman, Stephen Inglis, P.-N. Roy, R. G. Melko, and A. Del Maestro, “Path-integral monte carlo method for Rényi entanglement entropies,” *Phys. Rev. E* **90**, 013308 (2014).
- ⁴⁴ David J. Luitz, Xavier Plat, Nicolas Laflorencie, and Fabien Alet, “Improving entanglement and thermodynamic Rényi entropy measurements in quantum monte carlo,” *Phys. Rev. B* **90**, 125105 (2014).
- ⁴⁵ Anushya Chandran, M. Hermanns, N. Regnault, and B. Andrei Bernevig, “Bulk-edge correspondence in entanglement spectra,” *Phys. Rev. B* **84**, 205136 (2011).
- ⁴⁶ Xiao-Liang Qi, Hosho Katsura, and Andreas W. W. Ludwig, “General relationship between the entanglement spectrum and the edge state spectrum of topological quantum states,” *Phys. Rev. Lett.* **108**, 196402 (2012).
- ⁴⁷ Wen-Wei Ho, Lukasz Cincio, Heidar Moradi, Davide Gaiotto, and Guifre Vidal, “Edge-entanglement spectrum correspondence in a nonchiral topological phase and kramers-wannier duality,” *Phys. Rev. B* **91**, 125119 (2015).
- ⁴⁸ G. Vidal, J. I. Latorre, E. Rico, and A. Kitaev, “Entanglement in quantum critical phenomena,” *Phys. Rev. Lett.* **90**, 227902 (2003).
- ⁴⁹ V. E. Korepin, “Universality of entropy scaling in one dimensional gapless models,” *Phys. Rev. Lett.* **92**, 096402 (2004).
- ⁵⁰ J. L. Cardy, “Entanglement entropy in extended quantum systems,” *Euro. Phys. J. B* **64**, 321–326 (2008).
- ⁵¹ Rajibul Islam, Ruichao Ma, Philipp M. Preiss, M. Eric Tai, Alexander Lukin, Matthew Rispoli, and Markus Greiner, “Measuring entanglement entropy in a quantum many-body system,” *Nature* **528**, 77–83 (2015).
- ⁵² Anushya Chandran, Vedika Khemani, and S. L. Sondhi, “How universal is the entanglement spectrum?” *Phys. Rev. Lett.* **113**, 060501 (2014).
- ⁵³ Pasquale Calabrese, Massimo Campostrini, Fabian Essler, and Bernard Nienhuis, “Parity effects in the scaling of block entanglement in gapless spin chains,” *Phys. Rev. Lett.* **104**, 095701 (2010).
- ⁵⁴ Artur K. Ekert, Carolina Moura Alves, Daniel K. L. Oi, Michał Horodecki, Paweł Horodecki, and L. C. Kwek, “Direct estimations of linear and nonlinear functionals of a quantum state,” *Phys. Rev. Lett.* **88**, 217901 (2002).
- ⁵⁵ Dmitry A. Abanin and Eugene Demler, “Measuring entanglement entropy of a generic many-body system with a quantum switch,” *Phys. Rev. Lett.* **109**, 020504 (2012).
- ⁵⁶ Yu-Chin Tzeng, Hsiang-Hsuan Hung, Yung-Chung Chen, and Min-Fong Yang, “Fidelity approach to Gaussian transitions,” *Phys. Rev. A* **77**, 062321 (2008).